Epithelial and neutrophil interactions and innate immune response to *Shigella* in a human intestinal enteroid-neutrophil co-culture

Jose M. Lemme-Dumit,[1] Michele Doucet,[2] Nicholas C. Zachos,[2]* and Marcela F. Pasetti[1,3]*

[1]Department of Pediatrics, Center for Vaccine Development and Global Health, University of Maryland School of Medicine, Baltimore, MD, USA.

[2]Department of Medicine, Division of Gastroenterology and Hepatology, Johns Hopkins University School of Medicine, Baltimore, MD, USA.

[3]Lead contact

*Corresponding authors:

Marcela F. Pasetti, Ph.D.
685 West Baltimore St.; HSF-I Room 480
Baltimore, MD 21201
Email: mpasetti@som.umaryland.edu
Phone: 410-706-2341; Fax: 410-706-6205

Nicholas C. Zachos, Ph.D.
720 Rutland Avenue; Ross Research Building Room 943
Baltimore, MD 21205
Email: nzachos1@jhmi.edu
Phone: 410-614-0128; Fax: 410-955-9677

Abstract

Polymorphonuclear neutrophils (PMN) respond rapidly to gastrointestinal inflammation and infection. Herein, we report the development of an *ex vivo* tissue co-culture model consisting of human primary epithelial cells and PMN, and an in-depth analysis of their physical and molecular interactions and coordinated responses to *Shigella.* Co-culture structure, barrier function, cell phenotype, cytokines production, cell-to-cell interaction, and innate immune responses were characterized in the presence or absence of *Shigella*. PMN embedded within human intestinal epithelium acquired a distinct phenotype through molecular and epithelial cell contact signals, increased IL-8 production, and transmigrated across the epithelial cell layer. Upon *Shigella* infection, co-cultured PMN and epithelial cells increased production and secretion of IL-6, and PMN rapidly transmigrated across the epithelial barrier and phagocytosed bacteria on the apical surface. The epithelial cell-PMN co-culture represents an advanced technology for mechanistic interrogation of gastrointestinal physiology, host-microbe interaction, innate immunity, and evaluation of preventive/therapeutic tools.

Introduction

The intestinal epithelium creates a physical and molecular barrier that protects the host from potentially damaging elements in the constantly changing outside environment. Epithelial barrier function is supported by a diverse population of underlying immune cells, which deploy a variety of host-defense mechanisms against harmful agents (Peterson and Artis, 2014). Coordinated signals resulting from microbial sensing, cell-to-cell contact, cytokines, and other chemical mediators determine the type and extent of responses of gut immune cells, balancing tissue homeostasis with effective anti-microbial function via inflammation.

Advances in understanding intestinal physiology, pathophysiology, and host immunity have traditionally relied on studies conducted in animal models (or animal tissue) and in traditional tissue culture systems using colon cancer cell lines. Animal models, including the use of mutant mouse strains, have contributed to the mechanistic understanding of the composition, function, regulatory processes, and operatives of immunity at the gut mucosa. Unfortunately, host restrictions limit the utility and value of animal models (Mestas and Hughes, 2004, Gibbons and Spencer, 2011). This is the case for many enteric pathogens for which small animals fail to recreate disease as it occurs in humans. Likewise, immortalized (transformed) cell lines (e.g., HT-29, Caco-2, and T84) do not reflect human physiological responses but rather the aberrant behavior of diseased cells (e.g., karyotype defects). These cell-line based cultures also lack the multicellular complexity of the human intestinal epithelium, which further reduces the reliability and significance of the data generated.

The establishment of human enteroids from Lgr5^{+} intestinal stem cells was a breakthrough in tissue culture technology (Barker et al., 2007). Since then, three-dimensional (3D) intestinal enteroids have been widely used as models to study human gut physiology and pathophysiology as well as host-microbe interactions (Zhang et al., 2014, Huang et al., 2015, Co et al., 2019). Not only do enteroids render a truer physiological representation of the human epithelium, but they also offer a practical and reliable system to probe mechanisms and

interventions at the gut mucosal interface. The 3D spheroid conformation can be adapted to produce a 2D monolayer configuration with enteroids seeded on a semipermeable membrane (i.e., Transwell insert) (Foulke-Abel et al., 2014, In et al., 2016a, Rajan et al., 2018). An important practical advantage to this simplified format is that it allows for direct and controlled access to the apical (mimicking the lumen) and basolateral side of the epithelial cells, thus facilitating experimental manipulation and evaluation of outcomes. Enteroid monolayers, which can be generated from any gut segment, can mimic the undifferentiated (crypt-like) and differentiated (villus-like) profile of the intestinal epithelial cells (i.e., absorptive enterocytes, goblet cells, enteroendocrine cells, and Paneth cells) (Noel et al., 2017) and display segment-specific phenotypic and functional attributes of the normal human gut (In et al., 2016b). To better recreate the cellular complexity of the gastrointestinal mucosal barrier, we devised a human primary cell co-culture system consisting of enteroid monolayers and macrophages seeded on the basolateral side (Noel et al., 2017). Studies using this enteroid-macrophage co-culture model demonstrated physical and cytokine/chemokine-mediated interactions between intestinal epithelial cells and macrophages in the presence of pathogenic *E. coli* (Noel et al., 2017, Noel et al., 2018). Aiming to expand this co-culture conformation to include other phagocytic cells, we established an *ex vivo* co-culture model containing intestinal epithelial cells and human primary polymorphonuclear neutrophils (PMN) facing the monolayers' basal membrane. The histological and functional features of this co-culture model, such as cell integration, PMN phenotype, PMN-epithelial cell physical and molecular interactions, and cell function were characterized. Coordinated epithelial and PMN anti-microbial response was examined using *Shigella* as model enteric pathogen. *Shigella* causes diarrhea and dysentery in humans by trespassing the colonic barrier via M cells and infecting epithelial cells, and this process involves massive recruitment of PMN (Sansonetti et al., 1996). The enteroid-PMN co-culture modeled the paradoxical role of PMN contributing to inflammation and controlling infection.

Results

Establishment of a PMN-enteroid co-culture and PMN-epithelial cell interaction. To interrogate PMN adaptation and function in the human gut, we established an enteroid-PMN co-culture model that contains human enteroid monolayers and peripheral blood isolated human PMN. A human enteroid-macrophage co-culture with similar configuration has been developed by our group (Noel et al., 2017). Human ileal 3D organoids derived from Lgr5^{+}-containing biopsies from healthy subjects were seeded upon the inner (upper) surface of a Transwell insert and allowed to grow until they reached confluency. PMN isolated from peripheral blood of healthy human adult volunteers and exhibiting a CD15^{+}CD16^{+}CD14^{-} phenotype (Gustafson et al., 2015) were seeded on the outer (bottom) surface of the insert (Figure 1A). Confocal immunofluorescence microscopy and H&E staining confirmed the co-culture's expected epithelial cell polarity with the brush border oriented towards the luminal side (apical compartment) and adherent PMN facing the basolateral side of the monolayer (Figure 1B). Interestingly, PMN rapidly mobilized from the bottom side of the insert (where they were seeded) towards the epithelium. Within 2h of being added to the monolayers, PMN migrated from the insert and through the insert's pores (Figure S1) and intercalated within the epithelial cells (Figures 1B, C). The migrating PMN could be retrieved and enumerated in the apical compartment media (Figure 1D). The addition of PMN to the enteroid monolayer increased epithelial permeability, as shown by reduction in transepithelial electrical resistance (TER); although the difference did not reach statistical significance (Figure 1E). Because human IL-8 promotes PMN recruitment (Metzemaekers et al., 2020), we examined the effect of exogenous IL-8 on the mobilization of PMN co-cultured with epithelial cells and on monolayer permeability. Apical treatment of monolayers with 100 ng/ml IL-8 increased PMN epithelial transmigration (1.8-fold) (Figure 1D) and barrier permeability; the PMN-induced decrease in TER became

statistically significant in the presence of IL-8 (Figure 1F). Importantly, IL-8 alone did not affect the permeability of monolayers (Figure 1F).

Since cell movement is influenced by molecular mediators, we next examined the presence of cytokines (pro- and anti-inflammatory) and chemoattractant molecules in tissue culture media collected from the apical and basolateral compartments of enteroid monolayers alone and of enteroid-PMN co-cultures. Basolateral levels of IL-8 produced by the PMN-containing enteroids were 10-fold higher as compared to IL-8 produced by the monolayers alone, while MCP-1 and TNF-α remained unaffected by addition of PMN (Figure 1G). Similarly, the presence of PMN did not affect apical secretion of MCP-1, TNF-α, and IL-8 (Figure 1G). Production of MCP-1 was distinctly polarized, with higher levels being released to the apical side of the epithelial barrier. IL-1β, IL-6, IL-10, IL-12p70, IFN-γ, and TGF-β1 were measured but determined to be below the limit of detection of the assay for each cytokine.

Taken together, these results demonstrate adequate engraftment of PMN on the basolateral side of the enteroid monolayer, rapid migration of PMN across the monolayer to the luminal side, PMN-induced basolateral secretion of IL-8, and membrane de-stabilization (increased permeability) by IL-8-enhanced PMN transepithelial movement.

The human intestinal epithelium environment determines PMN immune phenotype and functional capacity. Cell phenotype, morphology, and function can be affected by the surrounding tissue and molecular environment. We hypothesized that the immune phenotype and functional capacity of PMN added to the enteroid monolayer would be influenced by their proximity or direct contact with the intestinal epithelium. To explore this hypothesis, we determined the expression of cell surface markers and phenotypic features of PMN isolated from peripheral blood in comparison with those of PMN within the enteroid co-culture. Two populations of co-cultured PMN were investigated following 2h of incubation: PMN residing

within the monolayer and in direct contact with the epithelial cells and PMN harvested from the basolateral media as tissue adjacent milieu (Figure 2A). PMN co-cultured with enteroid monolayers had a distinct phenotypic profile as compared with PMN obtained from peripheral blood. Regardless of their location, PMN co-cultured with enteroid monolayers exhibited increased expression of CD18 (β2 integrin), a molecule that participates in extravasation of circulating PMN, as well as upregulation of CD47, a receptor for membrane integrins involved in cell adhesion and migration, and of CD88 (C5a receptor), a molecule that mediates chemotaxis, granule enzyme release, and super anion production (Figure 2B; Figure S2B). CD66b, a marker of secondary granule exocytosis was likewise increased, but only in PMN harvested from the basolateral media (not in contact with cells) (Figure 2C; Figure S2B). In contrast, expression of CD182 (CXCR2 or IL-8RB) was reduced in all PMN added to co-culture, without distinction of retrieving site (Figure 2C; Figure S2B). PMN residing in close contact with epithelial cells exhibited increased expression of CD15 (E-selectin), a molecule that mediates PMN extravasation; CD16 (FcγRIII), a receptor for IgG that mediates degranulation, phagocytosis, and oxidative burst; and CD11b (α integrin), a protein that facilitates PMN adhesion and, along with CD18, forms the Mac-1 complex implicated in multiple anti-microbial functions (e.g., phagocytosis, cell-mediated cytotoxicity, cellular activation) (Figure 2D; Figure S2B). These results demonstrate that PMN within the intestinal epithelial environment undergo unique phenotypic adaptations, some of which are driven by molecular signals while others require direct PMN-epithelial cell contact.

PMN interaction with *Shigella* as a model enteric pathogen. To interrogate human epithelial cell and PMN interactions in the context of an enteric infection, we exposed the co-culture to wild type *Shigella flexneri* 2a (strain 2457T) as a model pathogen. PMN participate in *Shigella* pathogenesis through secretion of pro-inflammatory cytokines and deploy anti-microbial

functions including phagocytosis, proteolytic enzymes, anti-microbial proteins, and neutrophil extracellular traps (NETs) production. We first determined baseline responses of peripheral blood PMN in the presence of *Shigella*. PMN phagocytosed FITC-labeled *S. flexneri* 2a 2457T within 10 min of exposure; bacterial phagocytosis increased over time (up to 1h tested) reaching a maximum effect at 30 min (Figure 3A). In parallel, the number of bacteria recovered from the culture supernatant of *Shigella*-exposed PMN decreased significantly within 30- and 60-min exposure, in comparison to the number of bacteria recovered from control wells containing *Shigella* alone (in the absence of PMN) resuspended in tissue culture media or media that had been exposed to PMN to control for any soluble bactericidal source (Figure 3B). PMN viability was not affected during the first 2h of *Shigella* exposure, but decreased significantly by 3h post infection (Figure 3C). *Shigella*-exposed PMN exhibited changes in cell morphology and motility; formation of pseudopodia (projections of the cell membrane that enable locomotion) was observed within 30 min post infection (Figure 3D). In the presence of *Shigella*, PMN also displayed dynamic amoeboid motility toward the bacteria, and released NETs evidenced by a thick, diffuse, and opaque weave of DNA and entrapped bacilli (Figure 3E). FITC-stained *Shigella* colocalized with PMN phagolysosome (Figure 3F). In addition, PMN upregulated production and secretion of IL-8 and IL-1β, which are key molecular mediators of *Shigella* pathogenesis, 2h post infection, while production of IL-6 and MCP-1 was downregulated; production of TNF-α was not affected (Figure 3G). IL-10, TGF-β1, and IFN-γ were also measured but were below the limit of detection of the assay. A principal component analysis (PCA) of PMN function, viability, and cytokine production revealed an association between PMN-mediated phagocytosis and bactericidal activity with IL-8, IL-1β, and TNF-α production as indicated by principal component 1 on a PCA plot (Figure 3H). These results showed that PMN anti-microbial responses against *Shigella* involved morphological changes, phagocytic activity, and modulation of inflammatory cytokines.

Coordinated epithelial cell and PMN responses to *Shigella* in the co-culture model. We interrogated PMN and epithelial cell interactions and coordinated responses to *Shigella* in the PMN-enteroid co-cultures (Figure 1A). PMN were added to the enteroid monolayer as described above, allowed to settle for 2h, and then apically exposed to wild type *S. flexneri* 2a (MOI=10) for another 2h. Non-exposed co-cultures served as controls. Consistent with our previous observation, PMN facing the basolateral side of the epithelial cells moved swiftly through the filter pores, traversed between the epithelial cells and across the monolayer, and protruded on the apical side. PMN basolateral-apical transmigration increased in the presence of *Shigella* (Figure 4A). PMN that traversed across the monolayer phagocytosed bacteria on the luminal surface as evidenced by confocal fluorescent microscopy (Figure 4B; $CD16^+$ PMN are stained in green, engulfed *S. flexneri* 2a in red; actin in white). The process created a hole in the otherwise confluent epithelium (Figure 4C). Addition of PMN to the enteroid monolayers enabled *Shigella* to reach the basolateral side, whereas in the absence of PMN, *Shigella* was unable to trespass the intact enteroid (Figure 4D). Reduced (1.3-fold) TER values were observed in the *Shigella*-exposed PMN-enteroid co-culture as compared with *Shigella*-exposed monolayers alone or the monolayer control (no PMN, no *Shigella*) (Figure 4E), consistent with loss of barrier function and tissue damage that allowed bacterial translocation.

We next examined cytokines produced by *Shigella*-infected and non-infected PMN-enteroid co-cultures. MCP-1, TNF-α, and IL-8 were detected in the apical and basolateral compartments, as described above. *Shigella* infection resulted in reduced apical production of MCP-1 and TNF-α by the co-cultured cells as well as in increased production of IL-6 and substantially reduced secretion of IL-8 basolaterally (Figure 4F). IL-6 was only detected in the infected cultures and exhibited a clear basolateral polarization (Figure 4F). Cultures were also tested for presence of IL-1β, which along with IL-8, are hallmarks of *Shigella* pathogenesis, but were not detectable.

Collectively, these observations demonstrate that *Shigella* infection causes active recruitment of PMN to the luminal side, which results in discernible damage of the enteroid monolayer that paradoxically enables *Shigella* penetration and basolateral infection; still PMN actively engulfed bacteria and increased production and secretion of inflammatory cytokines to the apical and basolateral sides, respectively.

Phenotypic changes in PMN co-cultured with epithelial cells in response to *Shigella* infection. Additional experiments were conducted to determine the phenotypic features of PMN co-cultured with epithelial cells upon *Shigella* infection. PMN co-cultured with intestinal epithelial cells and exposed to *Shigella* exhibited increased expression of CD88, CD47, and CD66b as compared with PMN in co-cultures that remained uninfected (Figure 5A; Figure S3). In contrast, CD15 and CD18 expression was decreased on PMN from *Shigella*-infected co-cultures (Figure 5B; Figure S3). CD16, CD11b, and CD182 remained unchanged (Figure 5C; Figure S3). These results suggest that PMN residing within the intestinal environment undergo immune phenotypic adaptation as a result of pathogen exposure consistent with increased anti-microbial function (i.e., activation and expression of molecules that facilitate chemotaxis and epithelial transmigration).

Discussion

Epithelial cells and innate phagocytic cells underlying the intestinal epithelium work synergistically, preventing the trespassing of harmful agents and deploying rapid and effective host defense mechanisms against pathogens. PMN are the first innate immune cells recruited in response to gastrointestinal tissue inflammation and infection and they play a critical role initiating host immune responses (Fournier and Parkos, 2012). Patients with neutrophil disorders are prone to recurrent microbial infection (Lekstrom-Himes and Gallin, 2000, Wortmann et al., 2020). We report in this manuscript the successful establishment of an *ex vivo*

primary human intestinal epithelial-PMN co-culture and results from a mechanistic interrogation of cell interactions and innate responses to *Shigella* as a relevant diarrhoeagenic pathogen.

Our group developed the first *ex vivo* human enteroid- and monocyte-derived macrophage co-culture model in a monolayer format (Noel et al., 2017). The same approach was used to produce the PMN-enteroid co-culture described herein. Differently from macrophages, which remained in the basolateral side of the monolayer (where seeded) and responded to luminal organisms by extending transepithelial projections between adjacent epithelial cells, PMN rapidly migrated from the basolateral side of the epithelial cell and across the monolayer via the paracellular space. Histological and confocal microscopy images revealed PMN crawling through the Transwell insert pores, embedding at the base of the epithelial cells, and emerging on the luminal side of the enteroid monolayer, all within a few hours of co-culture. While macrophages contributed to cell differentiation and stabilized the epithelial barrier in our previous studies, PMN transmigration resulted in increased barrier permeability that enabled bacteria invasion. Intestinal epithelial repair events (e.g., cell proliferation and migration, and closure of leaking epithelial lateral spaces) reportedly begin minutes after acute mucosal barrier injury (Blikslager et al., 2007). As a corollary of these observations, we are investigating epithelial repair subsequent to PMN-induced inflammation and cell disruption, and the mechanisms and elements involved.

The capacity of PMN to migrate across the vascular endothelium (Sullivan et al., 2018) and a variety of tissues (Lammermann et al., 2013, Uderhardt et al., 2019), including epithelial cell layers (Sumagin et al., 2014, Parkos et al., 1991, Brazil et al., 2013, Flemming et al., 2018) has been documented *in vivo* (mainly in animal models) or *in vitro* using cell lines. These processes have been associated with PMN activation as a result of microbial sensing, inflammation, or danger signals. The level of myeloperoxidase (MPO), one of the principal enzymes contained in PMN granules and released upon activation, in stool is, in fact, a biomarker of inflammatory bowel disease severity (Masoodi et al., 2012). In our human PMN

and intestinal epithelial cell co-culture model, PMN migrated even in the absence of external stimulatory signals. PMN are not typically present in the homeostatic gut but actively recruited by signs of inflammation or infection (Kolaczkowska and Kubes, 2013); therefore, unprovoked PMN migration would not be expected. From the technical standpoint, the 3.0 μm pore size Transwell membrane used in our model allowed not only for successful and consistent growth of enteroid monolayers, but also the basolateral-to-apical migration of PMN; this system is more practical than the traditional growing of epithelial cells in an inverted manner, typically used for cancer cell lines.

The tissue microenvironment can influence immune cell phenotype and effector function capabilities (Grunwell et al., 2019, Svedberg et al., 2019). PMN from peripheral blood exhibited rapid phenotypic changes when incubated with enteroid monolayers. They acquired an activated phenotype that was triggered by tissue-derived signals. Compared to the PMN from peripheral blood, PMN co-cultured with epithelial cells had increased expression of CD18, which favors cell binding, of CD88, which is the receptor for C5a and facilitates degranulation and chemotaxis, and of CD47, a cell surface glycoprotein that supports transmigration across endothelial and epithelial cells (Vainer et al., 2000, Liu et al., 2001, Parkos et al., 1996). PMN phenotypic changes were influenced by their spatial location, i.e., whether they were in direct contact with epithelial cells or simply present in basolateral culture media. PMN in close proximity with the epithelium (the migratory PMN) had upregulated expression of CD15, which participates in chemotaxis and extravasation from circulation, as well as FcγRIII (CD16), a low affinity Fc receptor for IgG, and CD11b, a marker of cell adhesion and anti-microbial function (phagocytosis, degranulation, oxidative burst) (Golay et al., 2019, Teschner et al., 2019). On the other hand, PMN retrieved from the basolateral media, and which had not been in contact with the epithelial layer, exhibited increased expression of CD66b, indicative of PMN activation and degranulation (Zhao et al., 2004). This is to our knowledge the first detailed description of

dynamic changes of PMN immune phenotype in a translationally relevant model of the human intestinal epithelium.

MCP-1/CCL2, a chemoattractant and enhancer of bacterial killing and survival of phagocytic cells and IL-8, a potent promoter of PMN migration and tissue infiltration (Altstaedt et al., 1996, Andrews et al., 2018), were abundantly produced by the ileal monolayers in our co-culture model. TNF-α, a recruiter and activator of phagocytic cells (Ruder et al., 2019) was also detected, albeit at lower levels. IL-8, a hallmark product of intestinal epithelial cells, was further sourced by the PMN within the co-culture and released to the basolateral media; *in vivo* this subepithelial surge of IL-8 excess likely contributes to PMN recruitment. Expression of MCP-1, IL-8, and TNF-α has been reported in intestinal tissue of healthy adults in steady state (Reinecker et al., 1995, Raqib et al., 1995).

Again, when comparing PMN- and macrophage-enteroid co-cultures in terms of cytokine production, clear differences in innate immune functions emerged; while macrophages contributed to high levels of IFN-γ and IL-6, these cytokines were not detected in co-cultures containing PMN. The models were therefore capable of discerning morphological as well as functional cell adaptation.

Shigella invades the human colon and rectal mucosa and causes severe inflammation, massive recruitment of PMN, and tissue destruction (Sansonetti et al., 1996). Bloody/mucous diarrhea (dysentery) with large numbers of PMN in stool are hallmarks of shigellosis (Kotloff et al., 2018).

Human intestinal enteroids can be infected with *Shigella* (Ranganathan et al., 2019, Koestler et al., 2019). Hence, our model was fitting to interrogate coordinated innate responses of epithelial cells and PMN to this enteric pathogen. *Shigella* added on the luminal surface of the monolayers increased basolateral-apical PMN migration. Early efflux of PMN into the colonic tissue has been observed during shigellosis in the infected rabbit loop model (Perdomo et al.,

1994b). *Shigella*-induced PMN transmigration had been reported *in vitro* using colonic T84 cells (Perdomo et al., 1994a). Sansonetti and colleagues had shown that *S. flexneri* lipopolysaccharide trancytosed to the basolateral side of T84 cells in the presence of human normal sera and enhanced adherence of subepithelial PMN through IL-8 signaling (Beatty and Sansonetti, 1997).

PMN transmigration across the intestinal monolayer in our co-culture model caused microscopically visible epithelial cell damage and created a conduit for bacterial invasion and possibly amplification of infection. This observation is consistent with focal breakdown of the epithelial cell surface attributed to PMN migration in various disease states including infectious enterocolitis (Yardley and Donowitz, 1977). Our findings challenge for the first time the notion that M cells are necessary for *Shigella* epithelial translocation and invasion, and hint that the infiltration and barrier disruption by PMN offer another mechanism by which *Shigella* and other invasive enteric pathogens access the host internal compartment. We are presently studying reverse transmigration of bacteria-loaded PMN (out of the lumen and back to the basolateral side) as a possible means to initiate adaptive immunity through cross-presentation. The model lends itself to study of molecules that reduce PMN activity in the context of enteric infections and could prevent intestinal injury and inflammation.

Although acting in a “brute force” manner, PMN deployed potent anti-microbial activity against *Shigella*. As expected, PMN from circulation phagocytosed *Shigella* rapidly and efficiently and entrapped bacteria into NET structures. PMN anti-microbial functions coincided with increased production of IL-8 and the pyroptosis-inducer IL-1β, and downregulation of IL-6 and MCP-1. Likewise, PMN embedded within the epithelial cells promptly mobilized upon sensing *Shigella* on the epithelial cell surface and exhibited robust phagocytic capacity. Intriguingly, IL-8 levels were reduced, IL-1β was absent, and IL-6 was increased in the infected PMN-epithelial co-culture as compared to non-infected. A reduction of IL-8 production had been

reported in *Shigella*-infected human colonic explants, which was ascribed to anti-inflammatory bacterial proteins or death of IL-8 secreting cells (Coron et al., 2009). Reduced levels of these inflammatory cytokines may also reflect a regulatory feedback to prevent further tissue damage. Heightened levels of IL-6 and reduced TNF-α during infection may suggest a protective epithelial mechanism after injury (Kuhn et al., 2014, Ye et al., 2006). In addition, IL-6 has been attributed a beneficial role in enhancing Th17-protective immunity against *Shigella* re-infection (Sellge et al., 2010). Because cytokines measured in the co-culture supernatant represent the total amount produced by diverse cell types, this readout is limited in its capacity to discern subtle differences between culture conditions.

The immune phenotype of PMN in the co-culture adapted again as a result of *Shigella* infection, with further increases in activation/granule-associated markers CD66b, CD88, and CD47. CD47 has been implicated in PMN paracellular migration through epithelial cells in response to bacterium-derived leukocyte chemoattractant N-formyl-methionyl-leucyl-phenylalanine, in a process that involves intracellular distribution and increased CD47 cell surface expression (Liu et al., 2001). CD47-deficient mice have increased susceptibility to *E. coli* as a result of reduced PMN trafficking and bacterial killing activity (Lindberg et al., 1996). This finding is consistent with our observed upregulation of CD47 in *Shigella*-exposed PMN, which is likely associated with PMN's anti-microbial activity. CD16 and CD11b expression were unaltered on PMN co-cultured with intestinal enteroids and exposed to *Shigella*, indicating a preserved phagocytic capacity, whereas extravasation and cell adhesion markers CD15 and CD18 were downregulated. It has been reported that CD47 expression increases gradually and modulates CD11b-integrin function and CD11b/CD18 surface expression on PMN, suggesting a regulatory mechanism between these molecules (Liu et al., 2001, Azcutia et al., 2020). Expression of CD47 is self-protective; it avoids clearance by phagocytic cells (Jaiswal et al., 2009). The exact role of CD47 expression on PMN during *Shigella* infection remains to be elucidated.

Human intestinal xenografts in immunodeficient mice have been used to model interactions of *Shigella* with the human intestine *in vivo*. The model failed to discern any role of PMN in ameliorating or exacerbating disease, but revealed larger intracellular bacteria in PMN-depleted mice; the authors conclude that while PMN may contribute to tissue damage, they are important in controlling bacteria dissemination. The combination of species, immunodeficient background, and impracticality are major confounders/limitations of this model (Zhang et al., 2001).

Our studies provided new insights on the close communication between PMN and epithelial cells, phenotypic and functional changes on PMN prompted by the gastrointestinal environment, and their coordinated responses to *Shigella* as a model gastrointestinal pathogen. The PMN-epithelial cell co-culture described here provides a translationally relevant *ex vivo* model to study human epithelial cell-PMN physiology and pathophysiology, as well as host cell interactions and innate responses to enteric organisms. This model could be useful to interrogate innate immune defense mechanisms to enteric pathogens and to support the development and evaluation of preventive or therapeutic tools.

Materials and methods

Human PMN isolation

Human peripheral blood was collected in EDTA tubes (BD Vacutainer) from healthy volunteers enrolled in University of Maryland Institutional Review Board (IRB) approved protocol #HP-40025-CVD4000, and methods were conducted in compliance with approved Environmental Health and Safety guidelines (IBC #00003017). PMN were obtained by Ficoll-Paque (PREMIUM solution, GE Healthcare Bio-Sciences AB, Sweden) gradient centrifugation following dextran (Alfa Aesar, USA) sedimentation (Staab et al., 2020). Contaminating erythrocytes were removed by hypotonic lysis. After washing, cells (>95% of PMN determined by flow cytometry and May-Grünwald-Giemsa stained cytopreps) were suspended in enteroid differentiation media (DFM)

without antibiotics and immediately used. Cell counting and viability were determined using Guava Viacount Flex Reagent (Luminex, USA) following the manufacturer's instruction and analyzed in Guava 8HT using Viacount software (Luminex, USA).

Tissue collection and enteroid generation

Human enteroid cultures were established from biopsy tissue obtained after endoscopic or surgical resection from healthy subjects at Johns Hopkins University under Johns Hopkins University IRB approved protocol #NA-00038329, as previously described (Sato et al., 2011). Briefly, enteroids generated from isolated intestinal crypts from ileal segments were maintained as cysts embedded in Matrigel (Corning, USA) in 24-well plates and cultured in Wnt3A containing non-differentiated media (NDM) (Staab et al., 2020). Multiple enteroid cultures were harvested with Culturex Organoid Harvesting Solution (Trevigen, USA), and small enteroid fragments were obtained by digestion with TrypLE Express (ThermoFisher) in 37°C water bath for 90 seconds. Enteroid fragments were resuspended in NDM containing 10 μM Y-27632 and 10 μM CHIR 99021 inhibitors (Tocris) (NDM+inhibitors). The inner surface of Transwell inserts (3.0 μm pore transparent polyester membrane) pre-coated with 100 μl of human collagen IV solution (34 μg/ml; Sigma-Aldrich, USA) were seeded with 100 μl of an enteroid fragment suspension, and 600 μl of NDM+inhibitors was added to the wells of a 24-well tissue culture plate and incubated at 37°C, 5% CO_2, as previously described (Staab et al., 2020). NDM without inhibitors were replaced after 48h, and fresh NDM was added every other day; under these conditions, enteroid cultures reached confluency in 14-16 days. Monolayer differentiation was induced by incubation in Wnt3A-free and Rspo-1-free DFM without antibiotics for 5 days (Noel et al., 2017). Monolayer confluency was monitored by measuring TER values with an epithelial voltohmmeter (EVOM^2; World Precision Instruments, USA). The unit area resistances (ohm*cm^2) were calculated according to the growth surface area of the inserts (0.33 cm^2).

PMN-enteroid co-culture

Differentiated enteroid monolayers seeded on Transwell inserts were inverted and placed into an empty 12-well plate. PMN ($5x10^5$ in 50 μl of DFM) were added onto the bottom surface of the inserts and cells were allowed to attach for 2h at 37°C, 5% CO_2 (inserts remained wet throughout this process). The inserts were then turned back to their original position into a 24-well plate, and DFM was added to the insert (100 μl) and into the well (600 μl). Approximately 45% of the total PMN remained attached to the Transwell insert. TER measurements were collected after 2h, allowing monolayer recovering.

***Shigella flexneri* 2a infection**

Shigella flexneri 2a wild type strain 2457T was grown from frozen stocks (-80°C) on Tryptic Soy Agar (TSA) (Difco BD, USA) supplemented with 0.01% Congo Red dye (Sigma-Aldrich) overnight at 37°C. Bacterial inoculum was made by resuspending single red colonies in sterile 1X PBS pH 7.4 (Quality Biological). Bacterial suspension was adjusted to the desired concentration (~$1x10^8$ CFU/ml) in advanced DMEM/F12 without serum. A bacterial suspension containing ~ $5x10^6$ CFU in 50 μl was added directly to PMN (for 10-60 min) or to the apical compartment of enteroid monolayers alone or PMN-enteroid co-culture (for 2h), a multiplicity of infection of 10 relative to 1 PMN.

PMN transmigration

Basolateral-to-apical PMN transmigration was quantified by measurement of PMN MPO using a commercial kit (Cayman Chemical, Ann Arbor, MI) as previously described (Parkos et al., 1992). The assay was standardized with a known number of human PMN. MPO activity in lysates of enteroid monolayer alone was negligible.

PMN phagocytosis

S. flexneri 2a cultures grown overnight as described above were washed, resuspended in sterile PBS and incubated with FITC (Sigma-Aldrich) (20 μg/ml) for 30 min at 37□C. The bacteria suspension was thoroughly washed and adjusted to ~10^8 CFU/ml in sterile PBS/glycerol (1:2), and stored at -80□C until used. The day of the assay, FITC-labeled *Shigella* was incubated with PMN-autologous human sera for 30 min at 37□C. Opsonized bacteria $5x10^6$ CFU was added to PMN suspension ($5x10^5$ cells) and incubated for 10, 30, and 60 min. Phagocytosis was measured by flow cytometry. External fluorescence was blocked with the addition of trypan blue, and the difference between MFI blocked and non-blocked samples was used to calculate % phagocytosis (Brouwer et al., 2008, Chaka et al., 1995).

H&E and immunofluorescence staining

PMN-enteroid co-culture cells were fixed in aqueous 4% paraformaldehyde (PFA; Electron Microscopy Sciences, USA) at room temperature (RT) for 45 min and then washed with PBS. For H&E staining, monolayers were kept for at least 48h in formaldehyde solution, then embedded in paraffin, sectioned, mounted on slides, and stained with H&E. For immunofluorescence, cells were permeabilized and blocked for 30 min at RT in PBS containing 15% FBS, 2% BSA, and 0.1% saponin (all Sigma-Aldrich, USA). Cells were rinsed with PBS and incubated overnight at 4□C with primary antibodies: mouse anti-CD16 (LSBio, USA), rabbit anti-*S. flexneri* 2a (Abcam, USA) diluted 1:100 in PBS containing 15% FBS and 2% BSA. Stained cells were washed with PBS and incubated with secondary antibodies: goat anti-mouse AF488, goat anti-rabbit AF594 (all ThermoFisher, USA) diluted 1:100 in PBS 1h at RT; phalloidin AF594 or AF633 (Molecular Probes, ThermoFisher) was included in this step for actin visualization. Cells were washed and mounted in ProLong Gold Antifade Reagent with DAPI (Cell Signaling Technology, USA) for nuclear staining and maintained at 4□C. Lysosome was

stained with LysoTracker™ Red DND-99 (ThermoFischer) following the manufacturer's instructions.

Immunofluorescence microscopy

Confocal imaging was carried out at the Confocal Microscopy Facility of the University of Maryland School of Medicine using a Nikon W1 spinning disk confocal microscope running NIS-Elements imaging software (Nikon). Images were captured with a 40X or 60X oil objective and settings were adjusted to optimize signal. Immunofluorescence imaging (Figure 3F) was carried out using EVOS FL Imaging systems (fluorescent microscope) at 40X objective lens. Images were collated using FIJI/ImageJ (NIH). Signal processing was applied equally across the entire image. Actin channel was arranged to white-grey color for contrast purpose.

Flow cytometry

Cell phenotype was determined using the following human specific monoclonal antibodies from BD Pharmingen: HI98 (anti-CD15, FITC-conjugated), M5E2 (anti-CD14, APC-conjugated), 3G8 (anti-CD16, PE/Cy7-conjugated), D53-1473 (anti-CD88, BV421-conjugated), and BioLegend: TS1/18 (anti-CD18, PE/Cy7-conjugated), ICRF44 (anti-CD11b, BV421-conjugated), 5E8/CXCR2 (anti-CD182, APC-conjugated), CC2C6 (anti-CD47, PE/Cy7-conjugated), HA58 (anti-CD54, APC-conjugated), G10F5 (anti-CD66b, Pacific Blue-conjugated). PMN were blocked with 2% normal mouse serum (ThermoFisher) for 15 min at 4□C. After washing, cells were resuspended in FACS buffer (PBS containing 0.5% BSA and 2 mM EDTA; all Sigma-Aldrich) and 100 µl of equal number of cells were dispensed in several tubes and stained with antibodies for 30 min at 4□C. Antibodies were used diluted 1:2 – 1:1,000; optional amount was determined by in-house titration. Cells were washed in FACS buffer and either analyzed or fixed in 4% PFA for 15 min at 4□C and analyzed the next day. Marker expression was analyzed in a

Guava 8HT using Guava ExpressPro software (Luminex, USA) or BD LSRII using FACSDiva software (BD Biosciences, USA) and analyzed with FlowJo software (v10, Tree Star).

Cytokine and chemokine measurements

Cytokines and chemokines were measured by electrochemiluminescence microarray using commercial assays (Meso Scale Diagnostic, USA) following the manufacturer's instructions. IFN-γ, IL-1β, IL-6, IL-10, IL-12p70, TNF-α, MCP-1, TGF-β1, and IL-8 were reported as total amount (pg) contained in the entire volume of apical (100 μl) and basolateral (600 μl) culture supernatants.

Statistical analysis

Statistical significances were calculated using the Student's *t*-test unpaired, one-way or two-way analysis of variance (ANOVA) with Tukey's post-test as appropriate. PCA was performed by selecting PC with eigenvalues greater than 1.0 (Kaiser rule). Plots and statistical tests were performed using Prism software v9 (GraphPad, San Diego, CA). Treatment comparisons included at least three replicates and three independent experiments. Differences were considered statistically significant at p-value ≤ 0.05. Exact p values are indicated in each Figure. Results are expressed as mean ± standard error of mean (sem).

Acknowledgements

The authors want to thank Dr. Mark Donowitz, for critical reading of the manuscript and Robin Barnes and Nancy Greenberg, Clinical Research Nurses at University of Maryland, for their assistance in obtaining peripheral blood samples. The authors would like to acknowledge the Integrated Physiology Core of the Hopkins Conte Digestive Disease Basic and Translational Research Core Center (NIH P30 DK-089502 to N.C.Z.) for providing human enteroids and

growth factor conditioned media and the University of Maryland School of Medicine Center for Innovative Biomedical Resources, Flow Cytometry Shared Service. This work was supported by NIH/NIAID P01AI125181 Immunology and Enteroid Cores, and 1R01AI117734-01 to M.F.P.

Author Contributions

J.M.L-D. designed and performed experiments, conducted data analyses and interpretation. M.D. provided initial assistance with enteroid monolayers. N.C.Z. and M.F.P. participated in experimental design, data analyses and interpretation, and supervised the study. J.M.L-D. and M.F.P. wrote the manuscript. All authors edited the manuscript.

Disclosures

The authors have no financial conflicts of interest.

References

Altstaedt, J., Kirchner, H. and Rink, L. (1996). Cytokine production of neutrophils is limited to interleukin-8. Immunology*, 89*, 563-8.

Andrews, C., McLean, M.H. and Durum, S.K. (2018). Cytokine tuning of intestinal epithelial function. Front. Immunol.*, 9*, 1270.

Azcutia, V., Kelm, M., Luissint, A.C., Boerner, K., Flemming, S., Quiros, M., Newton, G., Nusrat, A., Luscinskas, F.W. and Parkos, C.A. (2020). Neutrophil expressed CD47 regulates CD11b/CD18-dependent neutrophil transepithelial migration in the intestine in vivo. Mucosal Immunol.*,* 10.1038/s41385-020-0316-4.

Barker, N., van Es, J.H., Kuipers, J., Kujala, P., van den Born, M., Cozijnsen, M., Haegebarth, A., Korving, J., Begthel, H., Peters, P.J., et al. (2007). Identification of stem cells in small intestine and colon by marker gene Lgr5. Nature*, 449*, 1003-7.

Beatty, W.L. and Sansonetti, P.J. (1997). Role of lipopolysaccharide in signaling to subepithelial polymorphonuclear leukocytes. Infect Immun*, 65*, 4395-404.

Blikslager, A.T., Moeser, A.J., Gookin, J.L., Jones, S.L. and Odle, J. (2007). Restoration of barrier function in injured intestinal mucosa. Physiol. Rev.*, 87*, 545-64.

Brazil, J.C., Liu, R., Sumagin, R., Kolegraff, K.N., Nusrat, A., Cummings, R.D., Parkos, C.A. and Louis, N.A. (2013). alpha3/4 Fucosyltransferase 3-dependent synthesis of Sialyl Lewis A on CD44 variant containing exon 6 mediates polymorphonuclear leukocyte detachment from intestinal epithelium during transepithelial migration. J. Immunol.*, 191*, 4804-17.

Brouwer, N., Dolman, K.M., van Houdt, M., Sta, M., Roos, D. and Kuijpers, T.W. (2008). Mannose-binding lectin (MBL) facilitates opsonophagocytosis of yeasts but not of bacteria despite MBL binding. J. Immunol.*, 180*, 4124-32.

Chaka, W., Scharringa, J., Verheul, A.F., Verhoef, J., Van Strijp, A.G. and Hoepelman, I.M. (1995). Quantitative analysis of phagocytosis and killing of Cryptococcus neoformans by human peripheral blood mononuclear cells by flow cytometry. Clin. Diagn. Lab. Immunol.*, 2*, 753-9.

Co, J.Y., Margalef-Catala, M., Li, X., Mah, A.T., Kuo, C.J., Monack, D.M. and Amieva, M.R. (2019). Controlling epithelial polarity: A human enteroid model for host-pathogen interactions. Cell Rep.*, 26*, 2509-2520.e4.

Coron, E., Flamant, M., Aubert, P., Wedel, T., Pedron, T., Letessier, E., Galmiche, J.P., Sansonetti, P.J. and Neunlist, M. (2009). Characterisation of early mucosal and neuronal lesions following Shigella flexneri infection in human colon. PLoS One*, 4*, e4713.

Flemming, S., Luissint, A.C., Nusrat, A. and Parkos, C.A. (2018). Analysis of leukocyte transepithelial migration using an in vivo murine colonic loop model. JCI Insight*, 3*, e99722.

Foulke-Abel, J., In, J., Kovbasnjuk, O., Zachos, N.C., Ettayebi, K., Blutt, S.E., Hyser, J.M., Zeng, X.L., Crawford, S.E., Broughman, J.R., et al. (2014). Human enteroids as an ex-vivo model of host-pathogen interactions in the gastrointestinal tract. Exp. Biol. Med. (Maywood)*, 239*, 1124-34.

Fournier, B.M. and Parkos, C.A. (2012). The role of neutrophils during intestinal inflammation. Mucosal Immunol.*, 5*, 354-66.

Gibbons, D.L. and Spencer, J. (2011). Mouse and human intestinal immunity: same ballpark, different players; different rules, same score. Mucosal Immunol.*, 4*, 148-57.

557 Golay, J., Valgardsdottir, R., Musaraj, G., Giupponi, D., Spinelli, O. and Introna, M. (2019).
558 Human neutrophils express low levels of FcgammaRIIIA, which plays a role in PMN
559 activation. Blood, *133*, 1395-1405.
560 Grunwell, J.R., Giacalone, V.D., Stephenson, S., Margaroli, C., Dobosh, B.S., Brown, M.R.,
561 Fitzpatrick, A.M. and Tirouvanziam, R. (2019). Neutrophil dysfunction in the airways of
562 children with acute respiratory failure due to lower respiratory tract viral and bacterial
563 coinfections. Sci. Rep., *9*, 2874.
564 Gustafson, M.P., Lin, Y., Maas, M.L., Van Keulen, V.P., Johnston, P.B., Peikert, T., Gastineau, D.A.
565 and Dietz, A.B. (2015). A method for identification and analysis of non-overlapping
566 myeloid immunophenotypes in humans. PLoS One, *10*, e0121546.
567 Huang, J.Y., Sweeney, E.G., Sigal, M., Zhang, H.C., Remington, S.J., Cantrell, M.A., Kuo, C.J.,
568 Guillemin, K. and Amieva, M.R. (2015). Chemodetection and destruction of host urea
569 allows Helicobacter pylori to locate the epithelium. Cell Host Microbe, *18*, 147-56.
570 In, J., Foulke-Abel, J., Zachos, N.C., Hansen, A.M., Kaper, J.B., Bernstein, H.D., Halushka, M.,
571 Blutt, S., Estes, M.K., Donowitz, M., et al. (2016a). Enterohemorrhagic Escherichia coli
572 reduce mucus and intermicrovillar bridges in human stem cell-derived colonoids. Cell.
573 Mol. Gastroenterol. Hepatol., *2*, 48-62 e3.
574 In, J.G., Foulke-Abel, J., Estes, M.K., Zachos, N.C., Kovbasnjuk, O. and Donowitz, M. (2016b).
575 Human mini-guts: new insights into intestinal physiology and host-pathogen
576 interactions. Nat. Rev. Gastroenterol. Hepatol., *13*, 633-642.
577 Jaiswal, S., Jamieson, C.H., Pang, W.W., Park, C.Y., Chao, M.P., Majeti, R., Traver, D., van
578 Rooijen, N. and Weissman, I.L. (2009). CD47 is upregulated on circulating hematopoietic
579 stem cells and leukemia cells to avoid phagocytosis. Cell, *138*, 271-85.
580 Koestler, B.J., Ward, C.M., Fisher, C.R., Rajan, A., Maresso, A.W. and Payne, S.M. (2019). Human
581 intestinal enteroids as a model system of Shigella pathogenesis. Infect. Immun., *87*,
582 e00733-18.
583 Kolaczkowska, E. and Kubes, P. (2013). Neutrophil recruitment and function in health and
584 inflammation. Nat. Rev. Immunol., *13*, 159-75.
585 Kotloff, K.L., Riddle, M.S., Platts-Mills, J.A., Pavlinac, P. and Zaidi, A.K.M. (2018). Shigellosis.
586 Lancet, *391*, 801-812.
587 Kuhn, K.A., Manieri, N.A., Liu, T.C. and Stappenbeck, T.S. (2014). IL-6 stimulates intestinal
588 epithelial proliferation and repair after injury. PLoS One, *9*, e114195.
589 Lammermann, T., Afonso, P.V., Angermann, B.R., Wang, J.M., Kastenmuller, W., Parent, C.A.
590 and Germain, R.N. (2013). Neutrophil swarms require LTB4 and integrins at sites of cell
591 death in vivo. Nature, *498*, 371-5.
592 Lekstrom-Himes, J.A. and Gallin, J.I. (2000). Immunodeficiency diseases caused by defects in
593 phagocytes. N. Engl. J. Med., *343*, 1703-14.
594 Lindberg, F.P., Bullard, D.C., Caver, T.E., Gresham, H.D., Beaudet, A.L. and Brown, E.J. (1996).
595 Decreased resistance to bacterial infection and granulocyte defects in IAP-deficient
596 mice. Science, *274*, 795-8.
597 Liu, Y., Merlin, D., Burst, S.L., Pochet, M., Madara, J.L. and Parkos, C.A. (2001). The role of CD47
598 in neutrophil transmigration. Increased rate of migration correlates with increased cell
599 surface expression of CD47. J. Biol. Chem., *276*, 40156-66.

600 Masoodi, I., Kochhar, R., Dutta, U., Vaishnavi, C., Prasad, K.K., Vaiphei, K., Hussain, S. and Singh,
601 K. (2012). Evaluation of fecal myeloperoxidase as a biomarker of disease activity and
602 severity in ulcerative colitis. Dig. Dis. Sci., *57*, 1336-40.
603 Mestas, J. and Hughes, C.C. (2004). Of mice and not men: differences between mouse and
604 human immunology. J. Immunol., *172*, 2731-8.
605 Metzemaekers, M., Vandendriessche, S., Berghmans, N., Gouwy, M. and Proost, P. (2020).
606 Truncation of CXCL8 to CXCL8(9-77) enhances actin polymerization and in vivo migration
607 of neutrophils. J. Leukoc. Biol., *107*, 1167-1173.
608 Noel, G., Baetz, N.W., Staab, J.F., Donowitz, M., Kovbasnjuk, O., Pasetti, M.F. and Zachos, N.C.
609 (2017). A primary human macrophage-enteroid co-culture model to investigate mucosal
610 gut physiology and host-pathogen interactions. Sci Rep, *7*, 45270.
611 Noel, G., Doucet, M., Nataro, J.P., Kaper, J.B., Zachos, N.C. and Pasetti, M.F. (2018).
612 Enterotoxigenic Escherichia coli is phagocytosed by macrophages underlying villus-like
613 intestinal epithelial cells: modeling ex vivo innate immune defenses of the human gut.
614 Gut Microbes, *9*, 382-389.
615 Parkos, C.A., Colgan, S.P., Delp, C., Arnaout, M.A. and Madara, J.L. (1992). Neutrophil migration
616 across a cultured epithelial monolayer elicits a biphasic resistance response
617 representing sequential effects on transcellular and paracellular pathways. J. Cell. Biol.,
618 *117*, 757-64.
619 Parkos, C.A., Colgan, S.P., Liang, T.W., Nusrat, A., Bacarra, A.E., Carnes, D.K. and Madara, J.L.
620 (1996). CD47 mediates post-adhesive events required for neutrophil migration across
621 polarized intestinal epithelia. J. Cell. Biol., *132*, 437-50.
622 Parkos, C.A., Delp, C., Arnaout, M.A. and Madara, J.L. (1991). Neutrophil migration across a
623 cultured intestinal epithelium. Dependence on a CD11b/CD18-mediated event and
624 enhanced efficiency in physiological direction. J. Clin. Invest., *88*, 1605-12.
625 Perdomo, J.J., Gounon, P. and Sansonetti, P.J. (1994a). Polymorphonuclear leukocyte
626 transmigration promotes invasion of colonic epithelial monolayer by Shigella flexneri. J.
627 Clin. Invest., *93*, 633-43.
628 Perdomo, O.J., Cavaillon, J.M., Huerre, M., Ohayon, H., Gounon, P. and Sansonetti, P.J. (1994b).
629 Acute inflammation causes epithelial invasion and mucosal destruction in experimental
630 shigellosis. J. Exp. Med., *180*, 1307-19.
631 Peterson, L.W. and Artis, D. (2014). Intestinal epithelial cells: regulators of barrier function and
632 immune homeostasis. Nat. Rev. Immunol., *14*, 141-53.
633 Rajan, A., Vela, L., Zeng, X.L., Yu, X., Shroyer, N., Blutt, S.E., Poole, N.M., Carlin, L.G., Nataro, J.P.,
634 Estes, M.K., et al. (2018). Novel segment- and host-specific patterns of
635 Enteroaggregative Escherichia coli adherence to human intestinal enteroids. mBio., *9*,
636 e02419-17.
637 Ranganathan, S., Doucet, M., Grassel, C.L., Delaine-Elias, B., Zachos, N.C. and Barry, E.M. (2019).
638 Evaluating Shigella flexneri pathogenesis in the human enteroid model. Infect. Immun.,
639 *87*, e00740-18.
640 Raqib, R., Lindberg, A.A., Wretlind, B., Bardhan, P.K., Andersson, U. and Andersson, J. (1995).
641 Persistence of local cytokine production in shigellosis in acute and convalescent stages.
642 Infect Immun, *63*, 289-96.

643 Reinecker, H.C., Loh, E.Y., Ringler, D.J., Mehta, A., Rombeau, J.L. and MacDermott, R.P. (1995).
644 Monocyte-chemoattractant protein 1 gene expression in intestinal epithelial cells and
645 inflammatory bowel disease mucosa. Gastroenterology, *108*, 40-50.
646 Ruder, B., Atreya, R. and Becker, C. (2019). Tumour necrosis factor alpha in intestinal
647 homeostasis and gut related diseases. Int. J. Mol. Sci., *20*.
648 Sansonetti, P.J., Arondel, J., Cantey, J.R., Prevost, M.C. and Huerre, M. (1996). Infection of
649 rabbit Peyer's patches by Shigella flexneri: effect of adhesive or invasive bacterial
650 phenotypes on follicle-associated epithelium. Infect. Immun., *64*, 2752-64.
651 Sato, T., Stange, D.E., Ferrante, M., Vries, R.G., Van Es, J.H., Van den Brink, S., Van Houdt, W.J.,
652 Pronk, A., Van Gorp, J., Siersema, P.D., et al. (2011). Long-term expansion of epithelial
653 organoids from human colon, adenoma, adenocarcinoma, and Barrett's epithelium.
654 Gastroenterology, *141*, 1762-72.
655 Sellge, G., Magalhaes, J.G., Konradt, C., Fritz, J.H., Salgado-Pabon, W., Eberl, G., Bandeira, A., Di
656 Santo, J.P., Sansonetti, P.J. and Phalipon, A. (2010). Th17 cells are the dominant T cell
657 subtype primed by Shigella flexneri mediating protective immunity. J. Immunol., *184*,
658 2076-85.
659 Staab, J.F., Lemme-Dumit, J.M., Latanich, R., Pasetti, M.F. and Zachos, N.C. (2020). Co-Culture
660 System of Human Enteroids/Colonoids with Innate Immune Cells. Curr Protoc Immunol,
661 *131*, e113.
662 Sullivan, D.P., Bui, T., Muller, W.A., Butin-Israeli, V. and Sumagin, R. (2018). In vivo imaging
663 reveals unique neutrophil transendothelial migration patterns in inflamed intestines.
664 Mucosal Immunol., *11*, 1571-1581.
665 Sumagin, R., Robin, A.Z., Nusrat, A. and Parkos, C.A. (2014). Transmigrated neutrophils in the
666 intestinal lumen engage ICAM-1 to regulate the epithelial barrier and neutrophil
667 recruitment. Mucosal Immunol., *7*, 905-15.
668 Svedberg, F.R., Brown, S.L., Krauss, M.Z., Campbell, L., Sharpe, C., Clausen, M., Howell, G.J.,
669 Clark, H., Madsen, J., Evans, C.M., et al. (2019). The lung environment controls alveolar
670 macrophage metabolism and responsiveness in type 2 inflammation. Nat. Immunol., *20*,
671 571-580.
672 Teschner, D., Cholaszczynska, A., Ries, F., Beckert, H., Theobald, M., Grabbe, S., Radsak, M. and
673 Bros, M. (2019). CD11b regulates fungal outgrowth but not neutrophil recruitment in a
674 mouse model of invasive pulmonary aspergillosis. Front. Immunol., *10*, 123.
675 Uderhardt, S., Martins, A.J., Tsang, J.S., Lammermann, T. and Germain, R.N. (2019). Resident
676 macrophages cloak tissue microlesions to prevent neutrophil-driven inflammatory
677 damage. Cell, *177*, 541-555 e17.
678 Vainer, B., Nielsen, O.H. and Horn, T. (2000). Comparative studies of the colonic in situ
679 expression of intercellular adhesion molecules (ICAM-1, -2, and -3), beta2 integrins (LFA-
680 1, Mac-1, and p150,95), and PECAM-1 in ulcerative colitis and Crohn's disease. Am. J.
681 Surg. Pathol., *24*, 1115-24.
682 Wortmann, S.B., Van Hove, J.L.K., Derks, T.G.J., Chevalier, N., Knight, V., Koller, A., Oussuren, E.,
683 Mayr, J.A., van Spronsen, F.J., Lagler, F.B., et al. (2020). Treating neutropenia and
684 neutrophil dysfunction in glycogen storage disease IB with an SGLT2-inhibitor. Blood,
685 10.1182/blood.2019004465, 2019004465.

686 Yardley, J.H. and Donowitz, M. (1977). Colo-rectal biopsy in inflammatory bowel disease.
687 Monogr Pathol, 50-94.
688 Ye, D., Ma, I. and Ma, T.Y. (2006). Molecular mechanism of tumor necrosis factor-alpha
689 modulation of intestinal epithelial tight junction barrier. Am. J. Physiol. Gastrointest.
690 Liver Physiol., *290*, G496-504.
691 Zhang, Y.G., Wu, S., Xia, Y. and Sun, J. (2014). Salmonella-infected crypt-derived intestinal
692 organoid culture system for host-bacterial interactions. Physiol. Rep., *2*, e12147.
693 Zhang, Z., Jin, L., Champion, G., Seydel, K.B. and Stanley, S.L., Jr. (2001). Shigella infection in a
694 SCID mouse-human intestinal xenograft model: role for neutrophils in containing
695 bacterial dissemination in human intestine. Infect. Immun., *69*, 3240-7.
696 Zhao, L., Xu, S., Fjaertoft, G., Pauksen, K., Hakansson, L. and Venge, P. (2004). An enzyme-linked
697 immunosorbent assay for human carcinoembryonic antigen-related cell adhesion
698 molecule 8, a biological marker of granulocyte activities in vivo. J Immunol Methods,
699 *293*, 207-14.
700

Figure legends

Figure 1. Establishment of a human PMN-enteroid co-culture. (**A**) May-Grünwald Giemsa image of PMN isolated from peripheral blood [left]. Representative dot plot of PMN phenotype [middle] and schematic representation the PMN-enteroid co-culture model [right]. (**B**) Confocal XZ projection [top; right, magnification XY projection] and H&E [bottom] images of the PMN-enteroid co-culture. Confocal: DNA, blue; actin, white; CD16 (PMN), green; Transwell insert, dashed lines. Arrowheads indicate PMN seeded on the Transwell insert and at the base of the columnar epithelium. (**C**) Representative immunofluorescence confocal microscopy image [top, XY; bottom, XZ projections] of the enteroid apical surface showing PMN intercalated and moving up within the epithelial cell monolayer. DNA, blue; CD16 (PMN), green; actin, white; Transwell insert, dashed line. (**D**) Number of PMN transmigrated to the luminal compartment 2h after being added to the co-culture in the absence or presence of apically delivered rhIL-8. (**E**) TER of enteroid monolayers and PMN-enteroid co-cultures in a 2h co-culture. (**F**) TER of enteroid monolayers and PMN-enteroid co-culture apically treated with rhIL-8 for 2h. (**G**) Total amount of cytokines secreted into the apical and basolateral compartments after 2h of co-culture. (D, E, F) Each dot represents the average from three replicate wells; data are shown as mean ± sem from 3 independent experiments. (G) Data are shown as mean + sem from 3 independent experiments in triplicate. *p* values were calculated by Student's *t*-test. See also Figure S1.

Figure 2. Distinctive phenotype of PMN within the human intestinal environment. (**A**) Schematic representation of PMN in direct contact with epithelial cells (C) or in the basolateral media (BM). (**B, C, D**) Phenotype of isolated PMN, PMN in C and BM determined by flow cytometry within 2h of co-culture. Each dot represents data collected from three replicate wells; data are shown as mean ± sem from 3 independent experiments. *p* values were calculated by one-way-ANOVA with Tukey's post-test for multiple comparisons. See also Figure S2.

Figure 3. Innate immune responses of human PMN to *S. flexneri*. (**A**) Representative confocal microscopy image and histogram of *S. flexneri* 2a-FITC uptake by human PMN. Confocal image [left, XY projection]. DNA, blue; actin, red; *S. flexneri* 2a, green. Histograms of PMN harboring *Shigella*-FITC [middle] and percentage of phagocytosis at 10, 30 and 60 min post infection [left]. Each dot represents the average from three replicates and PMN from 5 individual donors; data are shown as mean ± sem from 3 independent experiments. (**B**) Extracellular *S. flexneri* 2a colony forming units (CFU) in culture media following PMN exposure to *S. flexneri* 2a ($1x10^8$ CFU/ml) for 30 and 60 min; controls included *S. flexneri* 2a in culture media or in PMN-conditioned media without PMN. Each dot represents the average from three replicates and PMN from 6 individual donors; data are shown as mean ± sem from 3 independent experiments. (A, B) *p* values were calculated by one-way ANOVA with Tukey's post-test for multiple comparisons. (**C**) PMN viability in the presence and absence of *S. flexneri* 2a. Data represents the average from three replicates and PMN from 3 individual donors; data are shown as mean ± sem from 3 independent experiments. (**D**) PMN morphology before (0 min) and after (30 min) exposure to *S. flexneri* 2a. (**E**) Confocal microscopy image [XY projection] of NETs 30 min after exposure to *S. flexneri* 2a. DNA, blue; actin, red; *S. flexneri* 2a, green. (**F**) Immunofluorescence image showing *S. flexneri* 2a-FITC colocalization in PMN lysosome. Arrowheads indicate bacteria intracellularly and within the lysosome compartment. (**G**) Total amount of cytokines secreted in culture supernatant of PMN alone and PMN exposed to *S. flexneri* 2a for 2h. Data are shown as mean ± sem from 3 independent experiments in triplicate. (C, G) *p* values were calculated by Student's *t* test. (**H**) Principal component analysis (PCA) plot of *Shigella*-exposure PMN v. PMN monoculture. Variables analyzed: phagocytosis, bactericidal activity, viability, IL-1β, IL-6, IL-8, TNF-α, and MCP-1 variables.

Figure 4. Coordinated innate immune response to *Shigella* by human intestinal epithelial cells and PMN. (**A**) Numbers of PMN transmigrated to the apical compartment of enteroid monolayers exposed or not to *S. flexneri* 2a for 2h. (**B and C**) Confocal microscopy images [B: top, XY; bottom, XZ projections; right, magnification] of PMN-enteroid co-culture infected with *S. flexneri* 2a for 2h. PMN: CD16 (B, green), CD15 (C, red); *S. flexneri* 2a (B, red; C, green); actin, white; nuclei, blue. White arrowheads indicate *S. flexneri* 2a. (**D**) CFU in the apical and basolateral media of enteroid and PMN-enteroid co-cultures apically exposed to *S. flexneri* 2a for 2h. (**E**) TER of enteroid and PMN-enteroid co-cultures exposed to *S. flexneri* 2a for 2h. (**F**) Total amount of cytokines in the apical and basolateral media of PMN-enteroid co-cultures exposed or not to *S. flexneri* 2a for 2h. (A, D, E) Each dot represents the average from three replicate wells; data are shown as mean ± sem from 3 (A, E) and 5 (D) independent experiments. *p* values were calculated by Student's *t*-test. (F) Data are shown as mean + sem from 3 independent experiments in triplicate. *p* values were calculated by Student's *t*-test.

Figure 5. Immune phenotype of PMN co-cultured with epithelial cells and exposed to *Shigella*. (**A, B, C**) Cell surface expression of CD15, CD16, CD11b, CD18, CD88, CD66b, CD47, and CD182 on PMN embedded in the enteroid monolayer (co-culture) exposed or not to *S. flexneri* 2a for 2h. Each dot represents data collected from three replicate wells; data are shown as mean ± sem from 3 independent experiments. *p* values were calculated by Student's *t*-test. See also Figure S3.

Figure 1

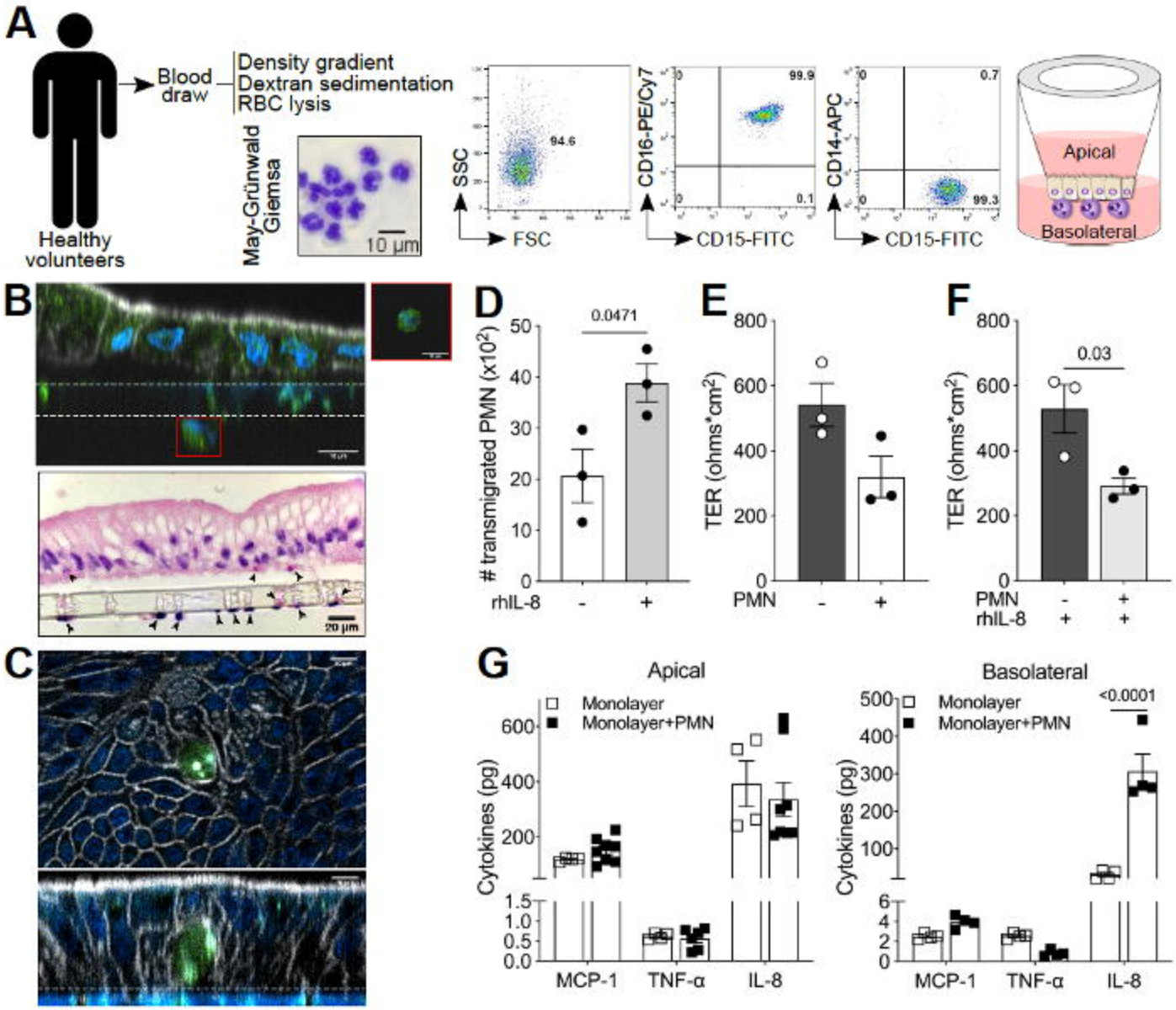
A
Healthy volunteers
Blood draw
Density gradient
Dextran sedimentation
RBC lysis
May-Grünwald Giemsa
10 µm
SSC
FSC
94.6
CD16-PE/Cy7
CD15-FITC
99.9
0.1
CD14-APC
CD15-FITC
0.7
99.3
Apical
Basolateral
B
20 µm
C
D
transmigrated PMN (x10²)
0.0471
rhIL-8
E
TER (ohms*cm²)
PMN
F
TER (ohms*cm²)
0.03
PMN
rhIL-8
G
Apical
Basolateral
Monolayer
Monolayer+PMN
Cytokines (pg)
<0.0001
MCP-1
TNF-α
IL-8

Figure 2

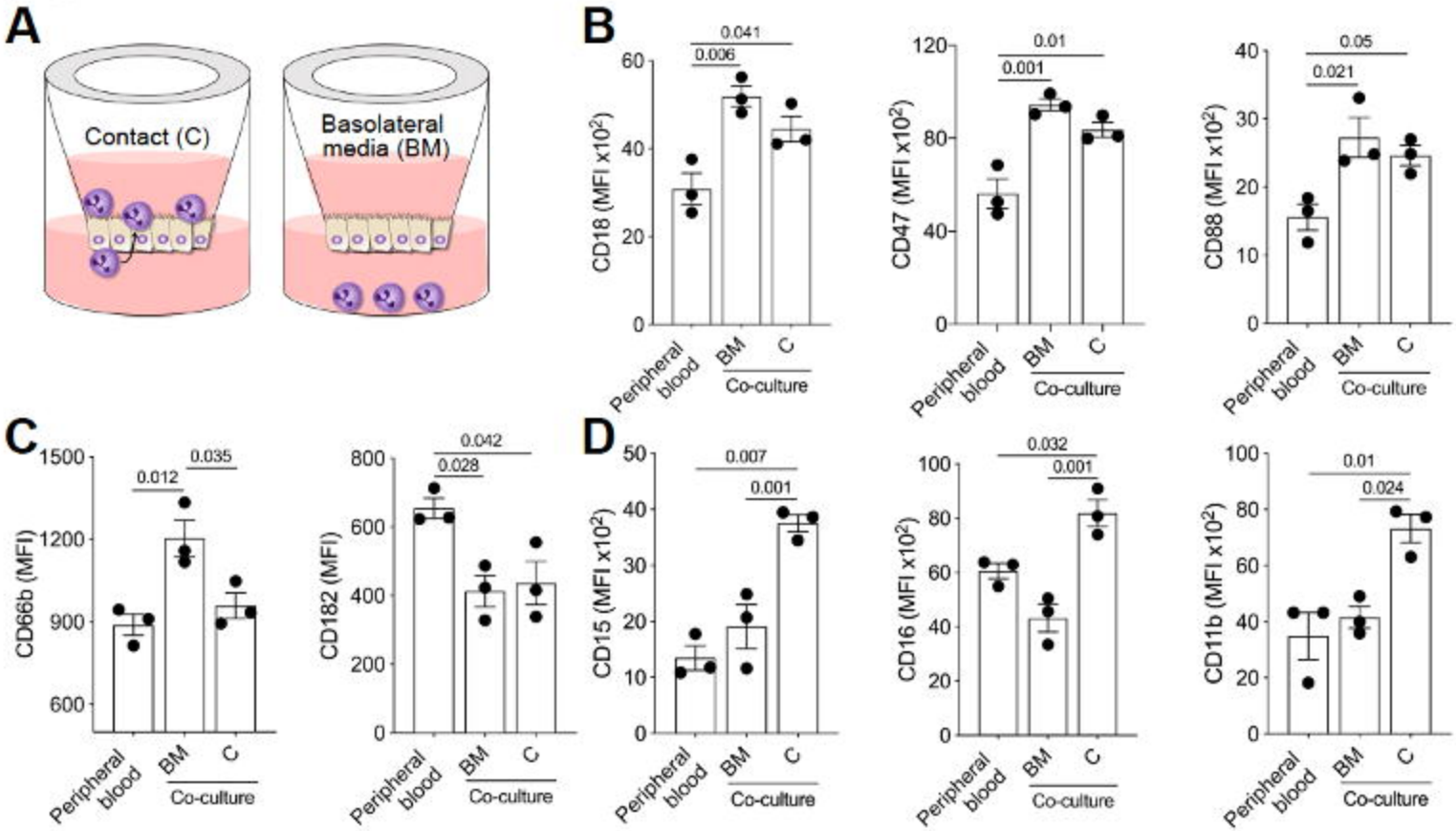
A
Contact (C)
Basolateral media (BM)
B
CD18 (MFI x10²)
0.041
0.006
CD47 (MFI x10²)
0.01
0.001
CD88 (MFI x10²)
0.05
0.021
C
CD66b (MFI)
0.012
0.035
CD182 (MFI)
0.042
0.028
D
CD15 (MFI x10²)
0.007
0.001
CD16 (MFI x10²)
0.032
0.001
CD11b (MFI x10²)
0.01
0.024
Peripheral blood
BM
C
Co-culture

Figure 3

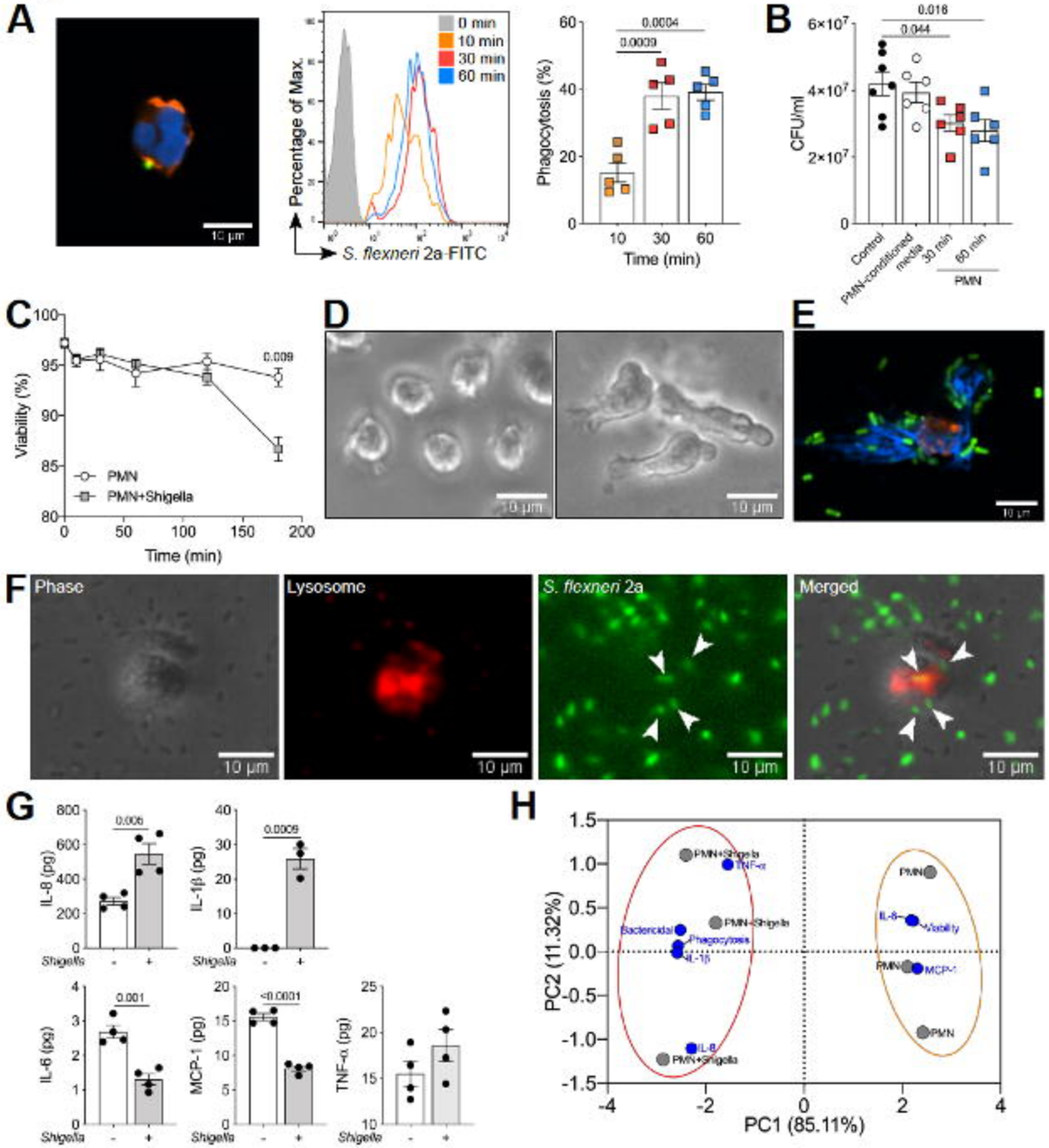
A
10 µm
0 min
10 min
30 min
60 min
Percentage of Max.
S. flexneri 2a-FITC
Phagocytosis (%)
Time (min)
0.0004
0.0009
B
CFU/ml
0.016
0.044
Control
PMN-conditioned media
30 min
60 min
PMN
C
Viability (%)
Time (min)
PMN
PMN+Shigella
0.009
D
E
F
Phase
Lysosome
S. flexneri 2a
Merged
G
IL-8 (pg)
IL-1β (pg)
IL-6 (pg)
MCP-1 (pg)
TNF-α (pg)
Shigella
0.006
0.0009
0.001
<0.0001
H
PC2 (11.32%)
PC1 (85.11%)
PMN+Shigella
TNF-α
Bactericidal
Phagocytosis
IL-1β
IL-8
PMN
Viability
MCP-1

Figure 4

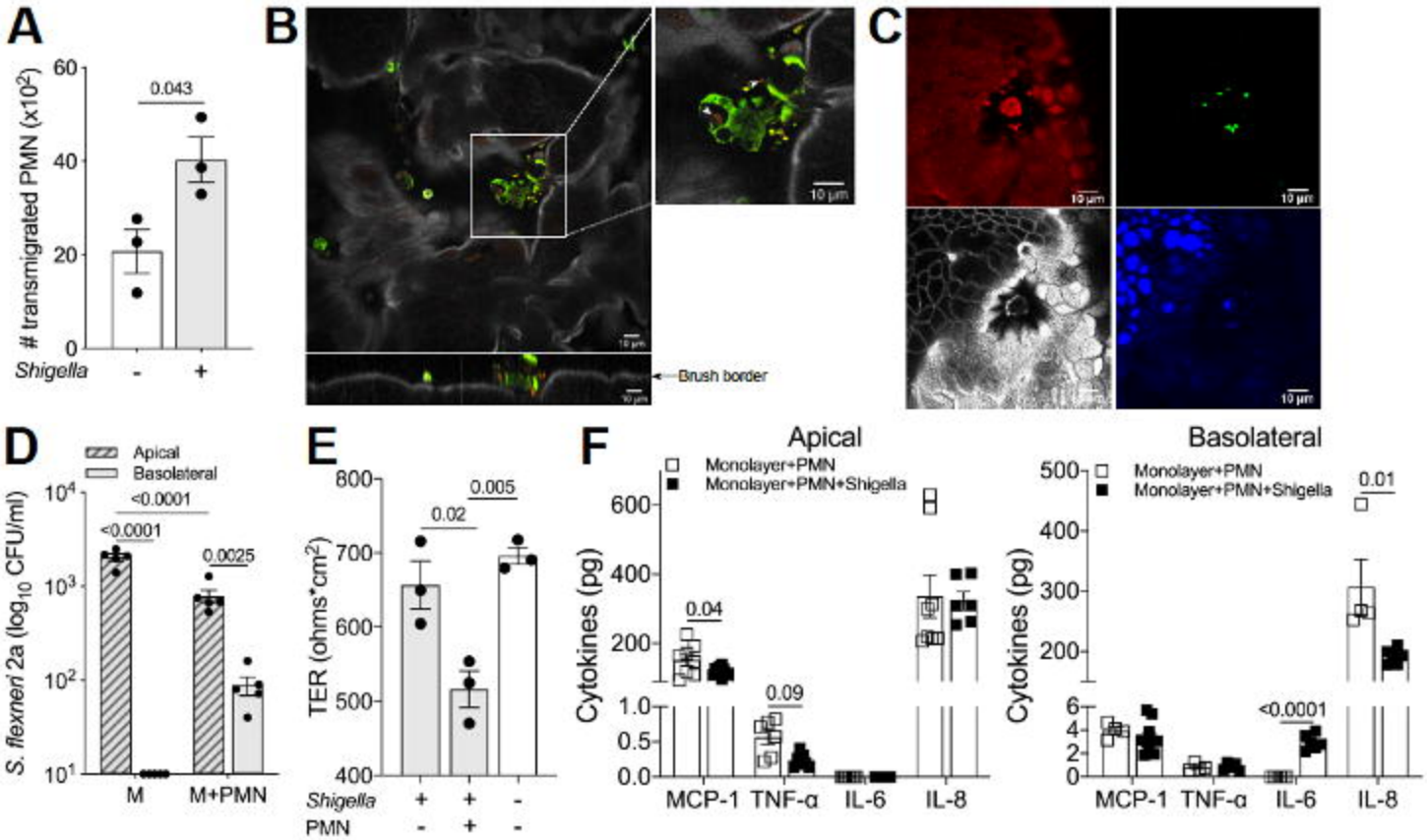
A
transmigrated PMN (x10²)
60
40
20
0
0.043
Shigella
-
+
B
Brush border
C
10 µm
D
Apical
Basolateral
S. flexneri 2a (log10 CFU/ml)
10⁴
10³
10²
10¹
<0.0001
<0.0001
0.0025
M
M+PMN
E
TER (ohms*cm²)
800
700
600
500
400
0.02
0.005
Shigella
PMN
F
Apical
Basolateral
Monolayer+PMN
Monolayer+PMN+Shigella
Cytokines (pg)
600
400
200
1.0
0.5
0.0
0.04
0.09
MCP-1
TNF-α
IL-6
IL-8
500
300
6
4
2
0
0.01
<0.0001

Figure 5

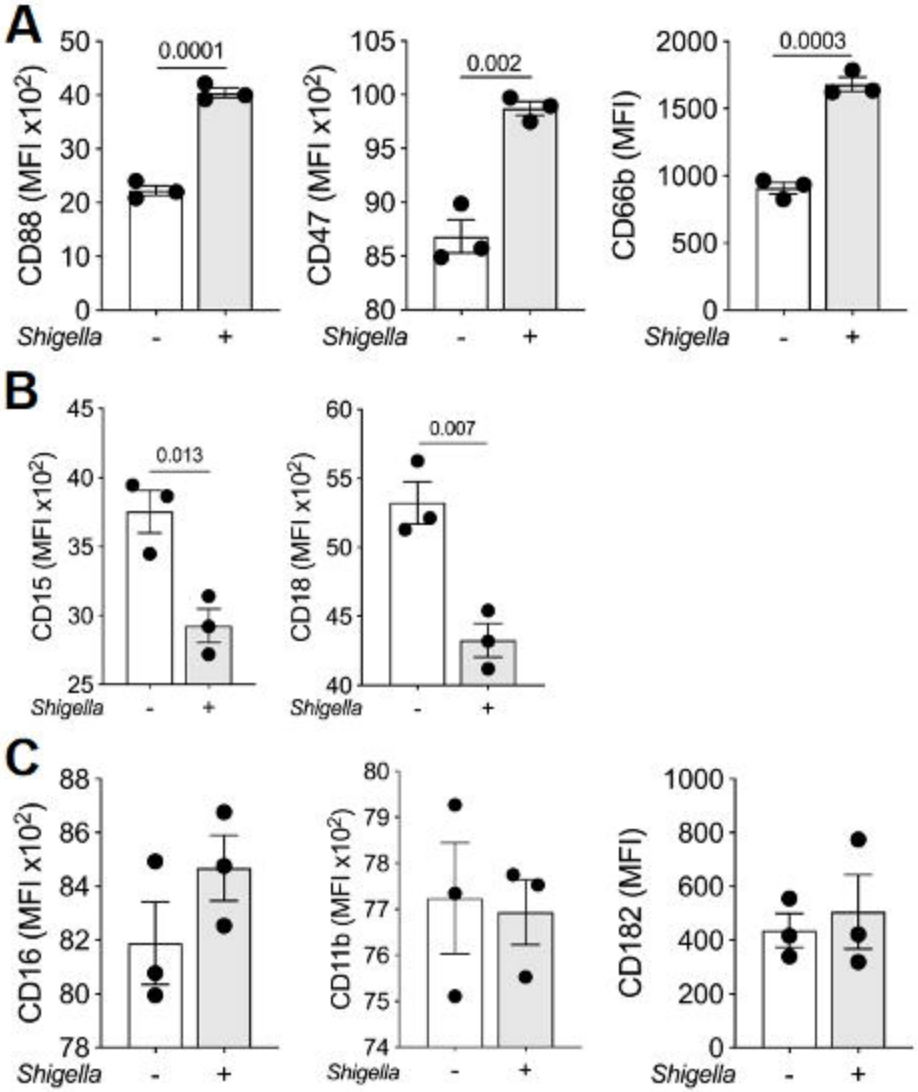
A
CD88 (MFI x10²)
0.0001
Shigella - +
CD47 (MFI x10²)
0.002
Shigella - +
CD66b (MFI)
0.0003
Shigella - +
B
CD15 (MFI x10²)
0.013
Shigella - +
CD18 (MFI x10²)
0.007
Shigella - +
C
CD16 (MFI x10²)
Shigella - +
CD11b (MFI x10²)
Shigella - +
CD182 (MFI)
Shigella - +